



Valorization of Furfural to Obtain High Value-Added Products with ZrO₂- and Al₂O₃-Pillared Clays

Salima Es Sih¹ · Francisco Franco-Duro¹ · Cristina García-Sancho¹ · Francisco José García-Mateos² · Juana María Rosas² · Ramón Moreno-Tost¹ · Pedro Maireles-Torres¹ · Juan Antonio Cecilia¹

Accepted: 3 May 2024
© The Author(s) 2024

Abstract

Two phyllosilicates (montmorillonite and saponite) have been selected as starting materials to synthesize ZrO₂- and Al₂O₃-pillared clays by the insertion of polyoxocations and subsequent calcination. These pillared clays display higher surface area, porosity and available acid sites in comparison to their respective raw clays. These samples were tested in the one-pot process to transform furfural into obtain valuable products. The incorporation of ZrO₂ allows to reach the highest furfural conversion values, with high yields towards furfuryl alcohol (FOL) at shorter reaction times, whereas the formation of *i*-propyl furfuryl ether (iPFE) is favored at longer times, attaining iPFE yields of about 50% after 24 h at 170 °C, using isopropanol as sacrificing alcohol.

Keywords Pillared clays · Furfural · One-pot reaction · Furfuryl alcohol · Alkyl furfuryl ether · Alkyl levulinate · γ -valerolactone

1 Introduction

The depletion of the fossil fuels has led to the search of alternative and sustainable resources to obtain chemicals and fuels, which are currently synthesized from fossil-based feedstocks [1, 2]. In this context, biomass has emerged as the most abundant and economical resource, and, in particular, lignocellulosic biomass is being the most studied for the production of high value-added chemicals [3]. Lignocellulose is mainly formed by three fractions: cellulose, hemicellulose and lignin, which can be isolated and then be subjected to biological and/or thermochemical processes to obtain their respective monomers, which can be transformed into valuable chemicals.

Focusing on the hemicellulose, this can be depolymerized by a hydrothermal treatment in acid medium to obtain liquors of its respective monomers, mainly xylose, which can be dehydrated to give rise to furfural (FUR) [4, 5]. FUR is

considered as a building block molecule due to it is possible to produce a large variety of products from hydrogenation, oxidation, condensation, amination reactions, among others [6]. Nevertheless, about 60–70% of the total production of FUR is used to obtain furfuryl alcohol (FOL) [7, 8] due to its high interest in the plastic and polymer fields by its high thermal resistance [9].

The hydrogenation reaction is been carried out industrially using copper chromite [6]. However, the high toxicity of Cr has driven research towards the development of alternative Cr-free catalysts, mainly based on Cu [10–13] or Ni as active phase [14–17]. Another alternative to reduce FUR into FOL is through the Meerwein-Ponndorf-Verley (MPV) reduction [18–20]. This process has been well known for more than 100 years; however, in the last decade, it has attracted the interest of the scientific community for the synthesis of FOL under mild conditions [21]. MPV process takes place through a catalytic transfer hydrogenation (CTH), where usually a secondary alcohol is used as sacrificing alcohol, which donates a hydrogen through a six-membered intermediate to reduce a carbonyl group of an aldehyde or ketone to the corresponding hydroxyl group, while the sacrificing secondary alcohol is oxidized to a ketone [21].

✉ Juan Antonio Cecilia
jacecilia@uma.es

¹ Departamento de Química Inorgánica, Cristalografía y Mineralogía, Universidad de Málaga, 29071 Málaga, Spain

² Departamento de Ingeniería Química, Universidad de Málaga, 29071 Málaga, Spain

Generally, the CTH reaction has been carried out in the presence of Lewis acid catalysts or basic catalysts [21], although the coexistence of Lewis and Brønsted acid sites can lead to consecutive reactions yielding valuable products, such as *i*-propyl levulinate (iPL) or γ -valerolactone GVL from FUR [21]. The first studies were performed using aluminum alkoxide [24, 25], and, more recently, heterogeneous catalysts have been tested for this reaction, which facilitate isolation of products and catalyst reuse. Among the heterogeneous catalysts studied in the CTH reaction, Al- [26, 27] and Zr-based [28–30] materials have been the most reported catalysts. In this sense, those catalysts where a small proportion of Zr has been structurally incorporated into porous silicas [31–33], zeolites [35–40], metal organic frameworks (MOFs) [41–43] or carbon [44–46] have demonstrated to be very active in CTH of FUR. Considering these results, it is necessary to synthesize more cheap catalysts for achieving a sustainable furfural hydrogenation process.

Clay minerals are very abundant in nature, being used in adsorption and catalytic processes. In addition, some phyllosilicates, like smectites, can host small molecules or cations in their interlayer region, even allowing the insertion of polyoxocations, whose thermal treatment gives rise to pillared clays (PILCs) [47, 48]. Thus, many studies have reported that smectites intercalated with inorganic species maintain meso- and microporosity after a thermal treatment above 300 °C [47]. In the present work, Al₂O₃ or ZrO₂ have been inserted in the form of polyoxocations into two smectites (montmorillonite and saponite). The presence of these metal oxides could improve the textural properties and the amount of acid sites, thus promoting the hydrogenation of FUR through CTH to obtain high value-added chemicals.

2 Materials and Methods

2.1 Reagents

Two smectites (montmorillonite and saponite), supplied by TOLSA, were used as starting materials for the preparation of the corresponding pillared clays. The Al-pillars were synthesized using aluminum nitrate nonahydrate, Al(NO₃)₃·9H₂O (Sigma-Aldrich, > 99%), while the Zr-pillars were formed using zirconium oxychloride octahydrate, ZrOCl₂·8H₂O (Sigma-Aldrich, 99%). Sodium hydroxide, NaOH > 99%, was supplied by VWR.

The catalytic process was carried out using furfural (Aldrich, > 98%), *o*-xylene (Aldrich, 99%), as the internal standard, and the solvent and sacrificing alcohol was 2-propanol (VWR, 99%).

The gases involved in the reaction, quantification of reagent and products and the characterization of the catalyst were He (Air Liquide, 99.999%), H₂ (Air Liquide, 99.999%),

N₂ (Air Liquide, 99.9999%) and N₂:O₂ (80:20% vol.) (Air Liquide 99.99%).

2.2 Synthesis of the Pillared Clays

The synthesis of Al-pillared clays was carried out following the methodology previously described in the literature [49, 50]. Briefly, a solution of NaOH 0.5 M was added dropwise to another solution of Al(NO₃)₃ 0.2 M, maintaining a OH/Al molar ratio of 2, obtaining the cation [AlO₄Al₁₂(OH)₂₄(H₂O)₁₂]⁷⁺. After 24 h stirring at room temperature, the pillaring solution was added dropwise to a 2 wt.% suspension of smectite. Then, the obtained suspension was aged at 60 °C for 6 h. The solid obtained after centrifugation was washed three times with distilled water. Finally, the solid was dried at 60 °C overnight and calcined at 400 °C for 2 h, with a heating rate of 2 °C/min.

Zr-pillared clays were obtained according to the methodology proposed previously [49, 51]. In this, a solution of ZrOCl₂ 0.1 M was added to a suspension of the smectite with a ratio of 1 mmol of Zr/g of smectite. The suspension was stirred at 60 °C for 24 h. Then, the solid was obtained after centrifugation and washed three times with distilled water. The final thermal treatment was similar to that of Al-pillared clays.

2.3 Characterization of the Catalysts

The starting clays and the pillared materials have been characterized by X-ray diffraction (XRD), attenuated total reflectance (ATR) FTIR spectroscopy, transmission electron microscopy (TEM), N₂ adsorption–desorption at –196 °C, NH₃ thermoprogrammed desorption (NH₃-TPD), pyridine thermoprogrammed desorption (Pyr-TPD), 2,6-dimethylpyridine desorption (2,6-DMPyr-TPD) and X-ray photoelectron spectroscopy (XPS).

The detailed information of the apparatus and the methodologies used for the analysis of the samples are compiled in the Supplementary Information.

2.4 Catalytic Tests

The hydrogenation of FUR was performed in Ace glass reactors, 15 mL of volume (Aldrich). Each test was carried out with 100 mg of catalyst, 0.1 mmol of FUR and 2-propanol, which was used as hydrogen donor, with a 2-propanol/FUR molar ratio of 50. In addition, 0.02 mL of *o*-xylene was added to the reaction medium as internal standard.

Before each test, the glass reactors were purged with He to minimize collateral reactions. The reaction was performed until a maximum time of 24 h with a temperature range between 130 and 170 °C, under magnetic stirring of 300 rpm. The temperature was controlled using a

thermocouple, directly in contact with an aluminum block, where the glass reactors were placed, which is directly heated with a heating plate with stirring.

The reuse studies were carried out under conditions like those described previously. Between each cycle, the catalyst was filtered and washed with the solvent (2-propanol). After that, the catalyst was dried at 100 °C overnight for later use in the next cycle.

Once the reaction is finished, the reactors were taken out of the aluminum block and cooled in water. Then, the liquid was microfiltered and analyzed by gas chromatography (GC), which was equipped a flame ionization detector (TCD) and a CP-Wax 52 CB capillary column using a heating rate of 2 °C/min from 40 °C to 200 °C, maintaining this temperature to 15 min. The analyzes were carried out in split mode.

The FUR conversion and yields of the products were determined as follows (Eq. 1 and Eq. 2):

$$\text{Conversion(\%)} = \frac{\text{moloffurfuralconverted}}{\text{moloffurfuralfed}} \times 100 \quad (1)$$

$$\text{Yield(\%)} = \frac{\text{molofproduct}}{\text{moloffurfuralfed}} \times 100 \quad (2)$$

3 Characterization of the Catalysts

The XRD patterns of the raw clays (Mont and Sap), compiled in Fig. 1, reveal that both phyllosilicates exhibit a broad diffraction peak, ascribed to the d_{001} reflection, with a maximum of 2θ of 7.0°, which corresponds to a layered structure with a basal spacing of 12.3 Å. This value is higher than that of a dry smectite (10 Å), which can be explained by the presence of cations, generally alkaline, in the inter-layer region to compensate the excess of negative charge in the phyllosilicate sheets. Furthermore, these cations are generally hydrated. In the same way, other typical diffraction peaks of smectites (d_{110} , d_{020} , d_{130} , d_{200} and d_{060}) can also be observed. Among them, the d_{060} reflection is very useful, since it allows to discern between dioctahedral and trioctahedral smectites. Thus, a dioctahedral smectite, like montmorillonite, displays a d_{060} reflection of $2\theta = 62.04^\circ$ (1.49 Å), while for trioctahedral smectites, like saponite, appears at $2\theta = 60.78^\circ$ (1.52 Å) [52]. In addition, minor amounts of crystalline quartz, gypsum and feldspars are also detected [52].

After the pillaring process, the basal diffraction (d_{001}) disappears in all cases, suggesting that the formation of a pillared structure causes the formation of a disordered, or delaminated phyllosilicates in the form of a house of cards, as previously described in the literature [53]. Moreover, it is also noteworthy that some impurities, mainly quartz, are still

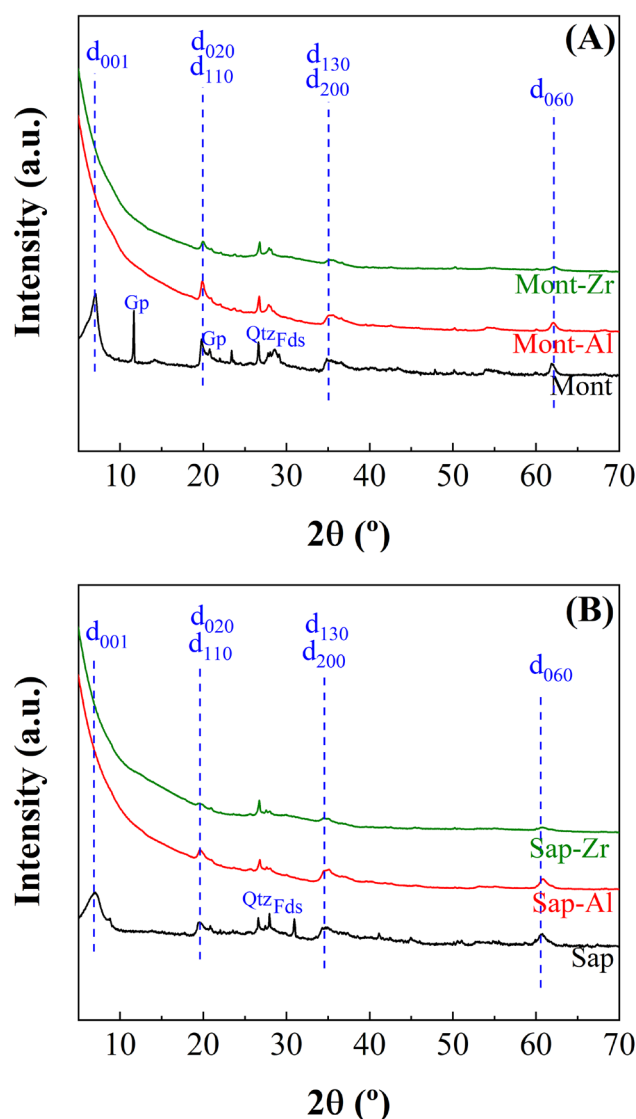


Fig. 1 X-ray diffraction patterns of Mont, Mont-Al and Mont-Zr (A) and Sap, Sap-Al and Sap-Zr (B). Notes. Gp: gypsum, Qtz: quartz, Fds: feldspar

observed after the pillaring treatment. On the other hand, no segregation phases of crystalline Al_2O_3 or ZrO_2 were detected by XRD after the pillaring process.

The morphology of the raw and modified clays was evaluated by TEM (Fig. 2). These micrographs evidence the lamellar structures of both Mont and Sap. However, these sheets have an anisotropic structure due to the genesis of these materials are subject to environmental effects. After the pillaring process, as previously noted, disordered and delaminated structures can be observed, mainly in those materials where Zr species has been incorporated. The study of the dispersion of Al and Zr species, after the pillaring step, by EDX mapping (Supplementary Information, Figures S1 and S2), would confirm the suitable dispersion of

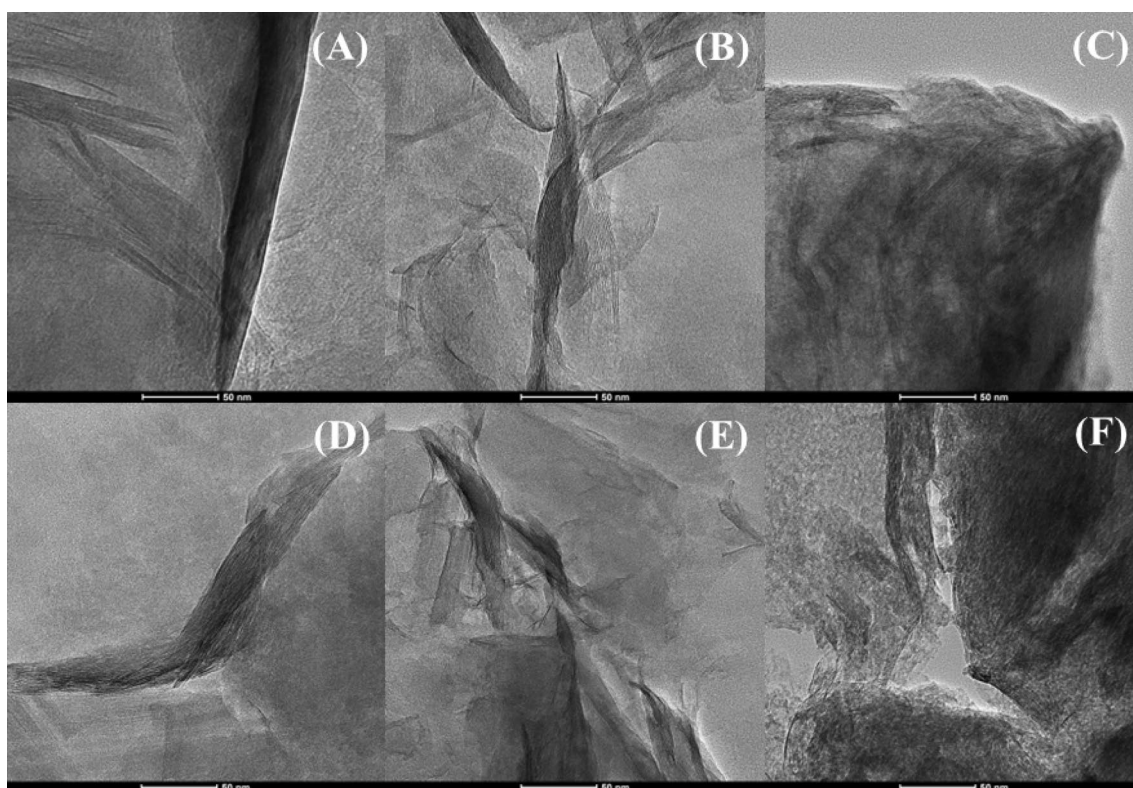


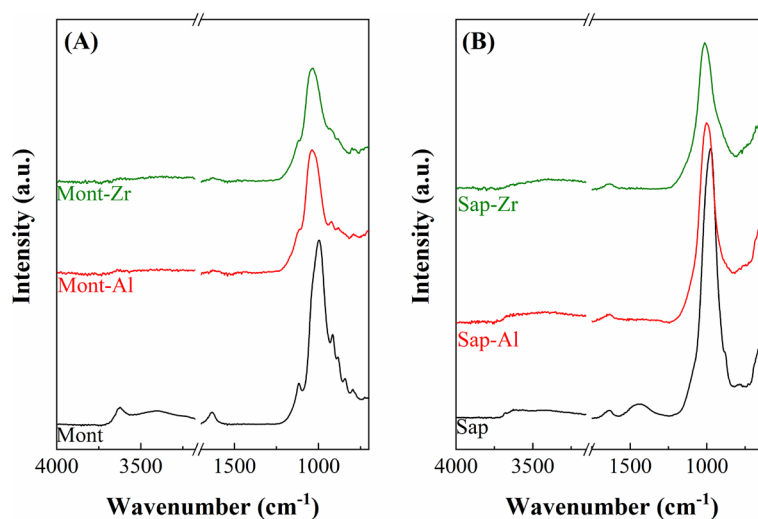
Fig. 2 TEM micrographs of Mont (A), Mont-Al (B), Mont-Zr (C), Sap (D), Sap-Al (E) and Sap-Zr (F). Scale: 50 nm

these species, discarding a segregation of Al_2O_3 or ZrO_2 phases, as was inferred by XRD (Fig. 1).

The structural characterization of the raw Mont and Sap was also carried out by ATR FTIR spectroscopy (Fig. 3). The OH stretching region, between 3750 and 3000 cm^{-1} , shows, for Mont, an absorption band located at 3625 cm^{-1} , which is attributed to stretching vibrations of OH forming $\text{Al}(\text{OH})\text{Al}$ linkages [54], confirming the presence of an Al-rich smectite, as montmorillonite. In the case of Sap, its

spectrum in the OH stretching region shows a less defined signal with a maximum located above 3680 cm^{-1} . This signal is assigned to OH stretching vibrations of $\text{Mg}(\text{OH})\text{Mg}$ -groups, which are typical of Mg-rich smectites, like saponite [55]. The Si–O stretching vibration appears about 980 cm^{-1} for both raw clays. In addition, other absorption bands are detected at lower wavenumber values. Thus, it has been previously reported that the bands located between 950 and 800 cm^{-1} can be attributed to Al-rich smectites, while the

Fig. 3 ATR FTIR spectra of Mont, Mont-Al and Mont-Zr (A) and Sap, Sap-Al and Sap-Zr (B)



bands between 700 and 600 cm^{-1} are assigned to Mg-rich smectites [56]. Finally, a small and broad band is observed between 1300–1600 cm^{-1} in the Sap sample [57], which is ascribed to low proportion of carbonate species, although crystalline metal carbonate were not detected by XRD.

Once the polyoxocations of Al and Zr have been incorporated and subsequently calcined to form nanoparticles of the corresponding metal oxides, acting as pillars in the interlayer region, the OH stretching region is modified, since the bands located between 3600 and 3700 cm^{-1} , which are ascribed to silanol groups, disappear. In this sense, the thermal treatment must cause a dehydroxylation in both phyllosilicates. On the other hand, the incorporation of Al and Zr species also provokes a shift of the Si–O stretching vibration at higher wavenumber values.

The determination of the textural properties was estimated from their N_2 adsorption–desorption isotherms at -196°C (Fig. 4). According to the IUPAC classification, the isotherms of the raw clay are between Types II and IV, which would imply that these solids display macroporosity ascribed to the voids between adjacent particles, but they also present a certain micro and mesoporosity [58], mainly in the case of the Sap sample where higher amount of N_2 is adsorbed at lower relative pressure. Moreover, the hysteresis loops can be considered as H3, which is found in non-rigid aggregates of plate-like particles, as those of Mont or Sap [58]. When Al or Zr species are incorporated in the interlayer region of these phyllosilicates, the isotherms evidence an increase in the N_2 adsorbed at low relative pressures, which results in an increase in microporosity, mainly in those materials where Zr species were incorporated.

The specific surface area of the materials has been calculated by the BET equation (Table 1) [59]. Raw Mont has a S_{BET} value of 47 m^2/g , while for Sap is 128 m^2/g . In this sense, the higher surface of Sap could be ascribed to its lower crystallinity, since this phyllosilicate displays less intense and broader diffraction peaks, as observed in Fig. 1. After the incorporation of Al and Zr species, S_{BET} values increase, although this improvement is more notable for

Table 1 Textural properties of the catalysts determined from N_2 adsorption–desorption isotherms at -196°C

Sample	S_{BET} (m^2/g)	S_{MIC} (m^2/g)	V_{P} (cm^3/g)	V_{MIC} (cm^3/g)
Mont	47	23	0.0505	0.0106
Mont-Al	93	78	0.0565	0.0316
Mont-Zr	237	212	0.1229	0.0867
Sap	128	81	0.1102	0.0365
Sap-Al	143	91	0.1160	0.0395
Sap-Zr	205	133	0.1394	0.0645

Zr-based materials, reaching the maximum value for Sap-Zr sample (237 m^2/g). This improvement of the textural properties is assigned to an increase in the meso- and, mainly, the microporosity by the formation of a pillared structure, as well as a partial delamination of the starting clays.

The study of the pore size distribution was carried out by DFT calculations (Fig. 5). Both raw phyllosilicates display a pore width with a maximum about 12 Å. After the incorporation of Al and Zr species in the phyllosilicates, a shift in the maximum of the pore width distribution at higher values is observed. This could confirm the formation of pillars in the interlayer region, although its deposition on the external surface cannot be ruled out. In the same way, the size distribution in the micropore region has also been studied for all samples (Fig. 6). The obtained data reveal that both raw clays (Mont and Sap) hardly display microporosity; however, the incorporation of Al and Zr species causes a different size pattern in both phyllosilicates. Thus, for Mont, a clear increase in the microporosity is observed, whereas, on the contrary, hardly affects the narrow microporosity of Sap.

Active sites for the CTH of FUR are associated to acid centers, so the determination of total acidity was evaluated by NH_3 -TPD (Table 2 and Supplementary Information, Figure S3). This study reveals that raw clays displays an acidity of 68 and 145 $\mu\text{mol}/\text{g}$ for Mont and Sap, respectively, being ascribed to the presence of silanol groups, but also to the presence of Al^{3+} or Mg^{2+} species located

Fig. 4 N_2 adsorption–desorption isotherms at -196°C of Mont, Mont-Al and Mont-Zr (A) and Sap, Sap-Al and Sap-Zr (B)

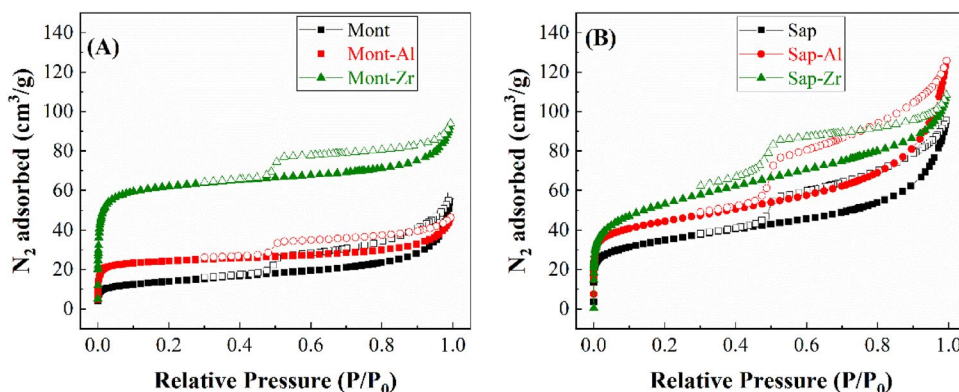


Fig. 5 Pore size distribution estimated by DFT method for Mont, Mont-Al and Mont-Zr (A) and Sap, Sap-Al and Sap-Zr (B)

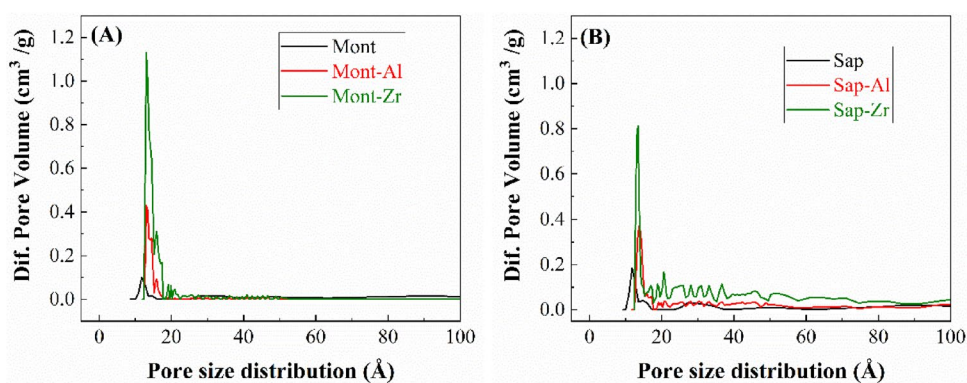


Fig. 6 Micropore width distribution estimated by MP method for Mont, Mont-Al and Mont-Zr (A) and Sap, Sap-Al and Sap-Zr (B)

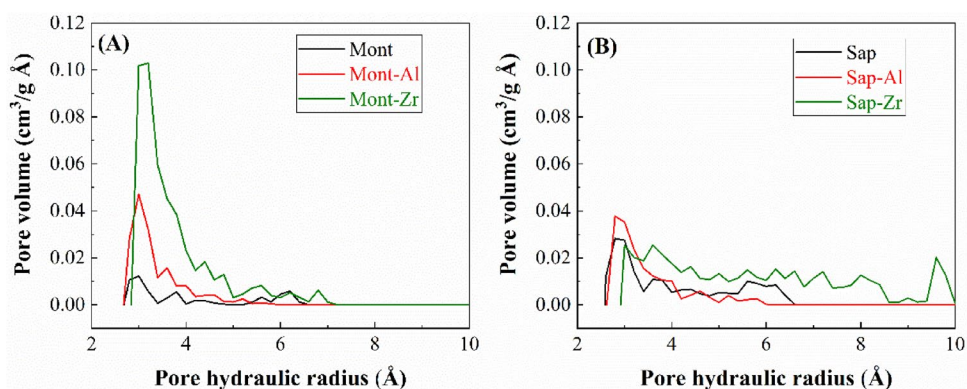


Table 2 Determination of the acid properties of the catalysts measured by NH_3 -TPD, Pyr-TPD and 2,6-DMPyr-TPD

Sample	NH_3 -TPD ($\mu\text{mol/g}$)	Pyr-TPD ($\mu\text{mol/g}$)	2,6-DMPyr-TPD ($\mu\text{mol/g}$)	(Pyr-TPD—2,6-DMPyr-TPD) ($\mu\text{mol/g}$)
Mont	60	28	6	22
Mont-Al	208	130	10	120
Mont-Zr	159	140	7	133
Sap	145	43	9	34
Sap-Al	159	70	10	60
Sap-Zr	435	160	20	140

in the octahedral sheets. The insertion of Al and Zr species in Mont or Sap causes a notable increase in the amount of acid sites in all cases, achieving values in the range of 159 and 435 $\mu\text{mol/g}$, respectively. The NH_3 -TPD data reveal that Sap-based catalysts display a higher acidity than those based on Mont, reaching the maximum value for the Sap-Zr catalyst (435 $\mu\text{mol/g}$).

In order to identify the nature (Lewis and/or Brønsted) of acid sites involved in the one-pot process of FUR conversion into valuable products, Pyr- and 2,6-DMPyr-TPD experiments were carried out (Table 2). In all cases, these values are below those obtained from NH_3 -TPD, which is expected,

since Pyr and 2,6-DMPyr are bigger molecules than NH_3 , in such a way that these molecules can suffer steric hindrance. The TPD of 2,6-DMPyr quantifies the amount of available Brønsted acid sites [60]. In all cases, the concentration of Brønsted acid sites is very low, reaching the highest value (20 $\mu\text{mol/g}$) for Sap-Zr. The Pyr-TPD provides information related to the sum of Brønsted and Lewis acid sites, so the difference between Pyr- and 2,6-DMPyr-TPD data provides the amount of Lewis acid sites. Lewis acidity predominates in all catalysts (Table 2). The incorporation of ZrO_2 and Al_2O_3 in both phyllosilicates increases the amount of Lewis acid sites compared to raw clays. Among them, Zr-based catalysts display a higher concentration of Lewis acid sites, achieving the highest value for Sap-Zr (140 $\mu\text{mol/g}$).

The analysis of the surface chemical composition of catalysts was performed by XPS (Table 3). As expected, Mont has a high Al content, while Mg is higher in Sap. These data confirm that Mont is a dioctahedral smectite, while Sap is trioctahedral, as was deduced by XRD (Fig. 1) and ATR FTIR spectroscopy (Fig. 3). The Si content is similar in both cases, with a surface content between 14.9 and 16.8%. On the other hand, the XPS results suggest that Na^+ is the main cation located in the interlayer region to counterbalance the charge deficiency of sheets. In all cases, the binding energy values are typical of phyllosilicates, such as montmorillonite and saponite.

Table 3 Surface atomic composition of the catalysts determined by XPS

Sample	Atomic concentrations							
	C 1 s	O 1 s	Si 2p	Al 2p	Mg 1 s	Zr 3d	Na 1 s	Fe 2p
Mont	16.0	57.2	16.8	5.7	1.4	–	1.9	1.0
Mont-Al	7.3	63.5	16.6	9.5	1.8	–	0.4	1.0
Mont-Zr	7.5	63.3	16.2	5.5	1.7	4.5	0.2	1.0
Sap	15.3	53.6	14.9	1.5	11.9	–	2.4	0.4
Sap-Al	9.0	58.3	15.0	5.3	11.4	–	0.6	0.4
Sap-Zr	10.0	58.8	14.5	1.7	8.79	5.2	0.1	0.4

After the formation of pillars, a decrease in carbon content is observed in all cases. This could suggest the presence of carbonate species in the raw clays, which are removed during the pillaring process. On the other hand, the incorporation of Al and Zr species causes an increase in the surface content of these cations of around 5% compared to raw smectites (Fig. 7). This confirms the incorporation of Zr or Al species after the pillaring process. Furthermore, the XPS data confirm that both Al and Zr appear in their oxide form. Finally, it is also noteworthy the decrease in the Na content, confirming that the Na⁺ ions are generally replaced by the Zr and Al polyoxocations, which are calcined to form nanoparticles of Al₂O₃ and ZrO₂, acting as pillars in the interlayer region of phyllosilicates.

4 Catalytic Results

Raw clays and pillared samples were evaluated as catalysts in the one-pot process of FUR conversion to valuable products. In this sense, it has been previously claimed that this one-pot process starts with the CTH reaction of FUR to obtain FOL. This reaction requires Lewis acid sites, and the mechanism takes place through a six-membered intermediate where a sacrificing alcohol, generally a secondary alcohol, transferred a hydrogen to an aldehyde or ketone, promoting its reduction. In the next step, FOL can be etherified with the sacrificing alcohol to yield iPFE, on Lewis or Brønsted acid sites. Then, both FOL and iPFE could suffer ring opening on Brønsted acid sites to produce alkyl levulinate, which is quickly reduced by a CTH reaction on Lewis acid sites via a lactonization process, forming GVL in the last step [34, 35].

In the first study, the catalytic activity of the raw clays was evaluated at 170 °C, which was selected according to previous works, since it is required for some steps involved in the one-pot process [21, 61–63] (Fig. 8). In both cases, FUR conversion increases with the reaction time, reaching a maximum conversion of 66% after 24 h with Sap, while it was only 52% for Mont. In spite of both catalysts possess a similar concentration of acid sites, as determined by Pyr-TPD, Sap has better textural (S_{BET} of 143 *versus* 47 m²/g)

and acid (145 *versus* 60 mol NH₃ desorbed/g) properties, which could explain its better catalytic performance.

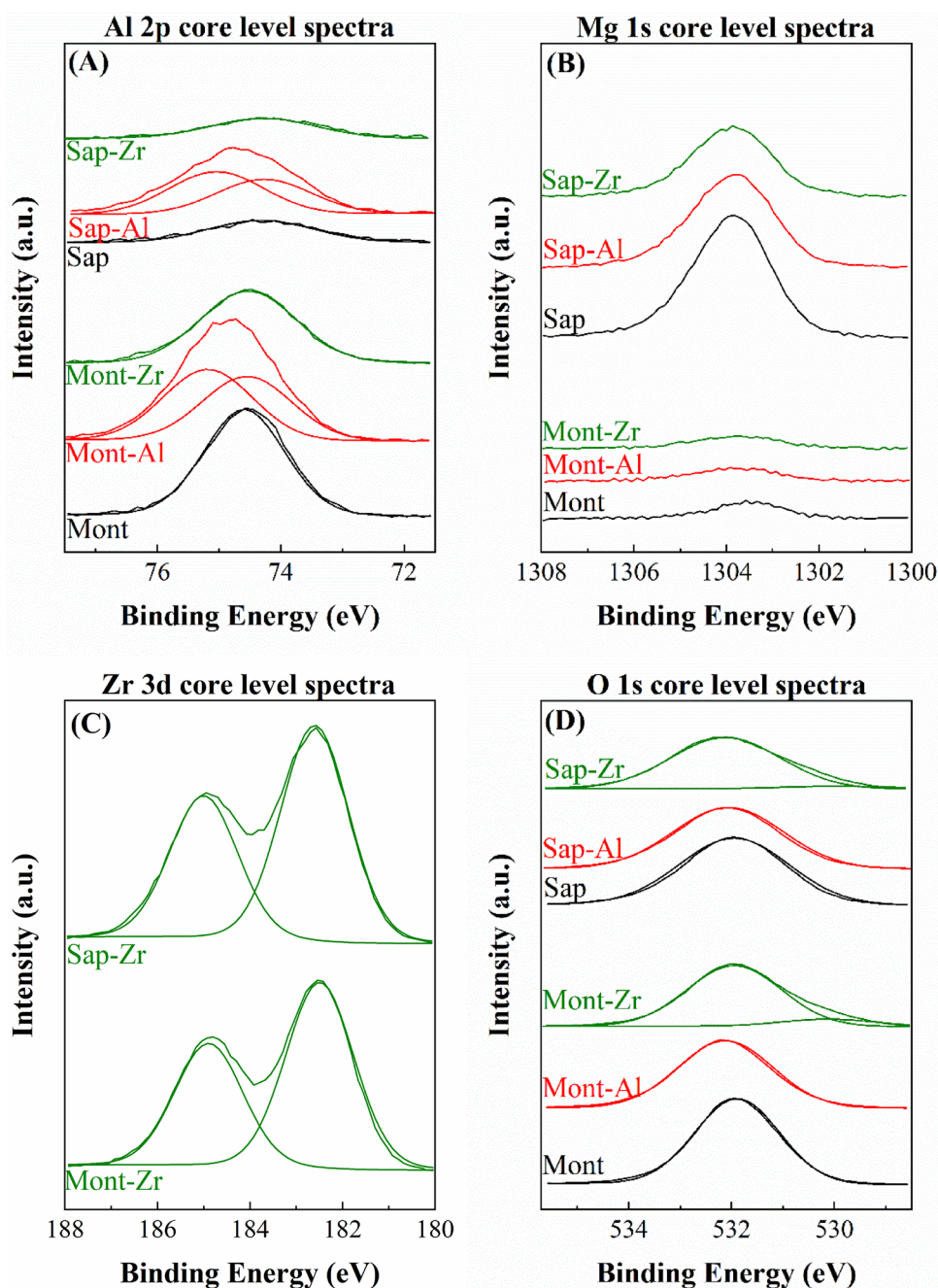
Regarding the reaction products, FOL is preferably formed at short reaction times with Mont, with a maximum yield of 15% after 6 h. At longer reaction times, a progressive decay in FOL yield is observed, which is accompanied by a rise of the iPFE and iPL yields, the last being the main product after 24 h, with a yield of 17%. It is also noteworthy that a yield of about 15% is associated to non-detected products. In the case of Sap, a similar trend is observed, since FOL is also obtained at short reaction times, decreasing with the reaction time. However, the yield pattern at longer reaction times differs from Mont, since Sap shows a lower proportion of iPL, the main product being iPFE, attaining a maximum value of 24% after 24 h. Moreover, the formation of non-detected products is also high, with a yield of 20%.

Next, the catalytic study of pillared clays (Fig. 9) revealed that, in all cases, FUR conversion was improved compared to raw clays. The incorporation of Al₂O₃ pillars in Mont or Sap led to lower FUR conversion values (Fig. 9A). These differences are even more pronounced at shorter reactions times. Thus, Mont-Al only reaches a FUR conversion of 13% after 1 h at 170 °C, while Sap-Al achieves a conversion of 33%, under similar experimental conditions. Longer reaction time causes an improvement in FUR conversion, attaining a value of 75% for Mont-Al and 86% for Sap-Al after 24 h. In the case of the Zr-based catalysts, the conversion values increase notably at shorter reaction time, since Mont-Zr reaches a value of 40% after 1 h, while Sap-Zr provides a conversion of 82%, with full conversion after about 6 h.

The higher FUR conversion attained with pillared clays could be ascribed to the incorporation of these metal oxides increases the amount of acid sites, which are involved in the consecutive reactions to obtain valuable products (Table 2). Between Al₂O₃ and ZrO₂, it has been previously reported that Zr(IV) species give rise to more active sites involved in the one-pot process of FUR [32, 34, 35, 42, 46].

Concerning the reaction products (Fig. 9B), FOL is again obtained at shorter reaction times. The incorporation of ZrO₂ to smectites leads to higher FOL yield, achieving a maximum value of 42% for Sap-Zr after 1 h, which agrees with the high activity in the MPV reaction of Zr-based catalysts

Fig. 7 Al 2p (A), Mg 1s (B), Zr 3d (C) and O 1s (D) core level spectra of the catalysts



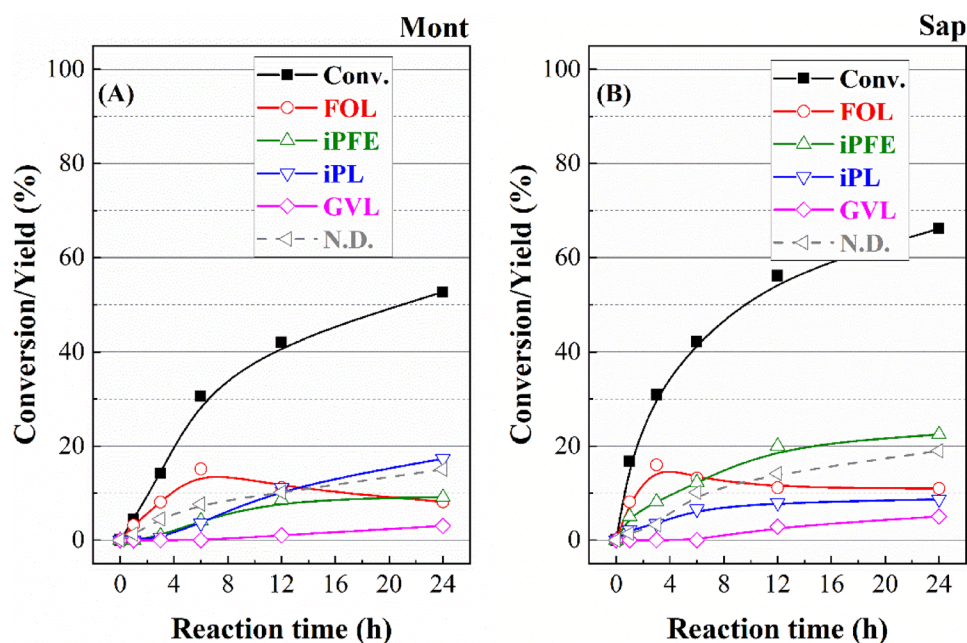
[37]. In this sense, the presence of Lewis acid sites in these catalysts promotes the catalytic transfer of hydrogen, as several authors have stated [21, 34, 35].

The use of longer reaction times again causes a progressive decrease in FOL yield, which is associated to the formation of iPF₂E (Fig. 9C). It has been previously reported that this step can be performed with the participation of Lewis or Brønsted acid sites [62]. The formation of iPF₂E is faster when ZrO₂ has been incorporated in the phyllosilicates. In both cases, yields close to 50% are reached for Mont-Zr and Sap-Zr after 12 h. However, those catalysts where

Al₂O₃ has been incorporated, Mont-Al and Sap-Al, display a more progressive increase in the iPF₂E yield, a maximum yield of 43% being attained with Sap-Al after 24 h. These data indicate that Zr-based catalysts, which are more active in the reaction, are also the catalysts most likely to favor etherification reactions with the sacrificial alcohol to form iPF₂E. Thus, several papers have reported that Al₂O₃-based catalysts are less prone to promote etherification reaction than ZrO₂-based ones [26, 34, 35].

On the other hand, the formation of iPL (Fig. 9D) is more progressive throughout the 24 h, although the

Fig. 8 FUR conversion and yield with raw Mont (A) and Sap (B). (Experimental conditions: 0.1 g of catalyst, temperature reaction: 170 °C, reaction time: 0–24 h, iPOH/FUR molar ratio: 50, FUR/catalyst weight ratio: 1)



maximum iPL yield is 24% with Mont-Al, while the rest of catalysts display yields below 16%. From these results, the one pot process seems to be retained in the formation of FOL or iPFE. This fact could be ascribed to the low proportion of Brönsted acid sites (Table 2), which are required for the opening of the furan ring to form alkyl levulinates [34]. Finally, small proportions of GVL are also observed (Fig. 9E), which is expected, since the one-pot process does not progress to more advanced consecutive reactions. In any case, it has been reported that the formation of GVL is the limiting step in the one-pot process, due to long reaction time and high temperature are required to promote the final lactonization to form GVL, through Lewis or Brönsted acid sites [34]. Thus, the maximum GVL yield is obtained for Sap-Zr, with 10% after 24 h.

In addition, the analysis of the carbon balance has revealed the formation of non-detected products (Fig. 9F), whose yields increase at longer reaction times, with values between 25 and 33% after 24 h.

Once the catalysts were tested in the CTH of FUR to obtain valuable products, the used catalysts were recovered to identify modifications of physico-chemical properties of the catalysts along the reaction. The analysis of the textural properties of the used catalysts, reported in Table 4, shows a drastic decrease in both mesoporosity and microporosity in all catalysts. A detailed study of the pore size distribution, determined by the DFT method (Supplementary Information, Figure S4), has confirmed a blockage of the pore with dimensions in the range of 1–2 nm. In this sense, previous studies have reported that FUR and FOL are prone to suffer polymerization reactions leading to humins or resins [64–66], which can be deposited in

the micro- and mesopores, worsening textural properties of catalysts.

The characterization of the catalysts after the reaction by XPS showed that the atomic concentration data differ compared to the fresh catalysts (Table 5). Thus, the surface C content increases markedly after the reaction, with percentages between 38.2 and 58.6%, which agrees with studies reported in other reactions of hemicellulose valorization [67].

However, the Si, Al, Mg and Zr contents decreases after the reaction (Supplementary Information, Figure S5). These data would point out the deposition of carbonaceous species on the catalyst surface, which causes a progressive blockage of the active sites involved in the reaction. In fact, the detailed analysis of the C 1s core level spectra (Fig. 10A) reveal the presence of C–O–C or C–O–H bonds (at a binding energy of 286.0 eV), which could confirm the deposition of furfural or furfuryl alcohol derivatives in the form of humins. In the same way, the O 1s core level spectra also display a new contribution located about 533 eV (Fig. 10B), which is ascribed to organic C–O bonds, also agreeing with the deposition of carbonaceous species.

In the next study, the influence of the reaction temperature on the CTH of FUR has been evaluated (Fig. 11). In the entire temperature range studied, the insertion of ZrO₂ nanoparticles in smectites led to a higher activity at lower reaction times. The highest FUR conversion was obtained for Sap-Zr, which achieves a FUR conversion of 81% after only 6 h at 130 °C, while it was almost complete after 6 h at 170 °C. Regarding the obtained products, FOL and iPFE are generally formed at lower temperature [31]. Among them, in most of cases, FOL yields decay when the temperature

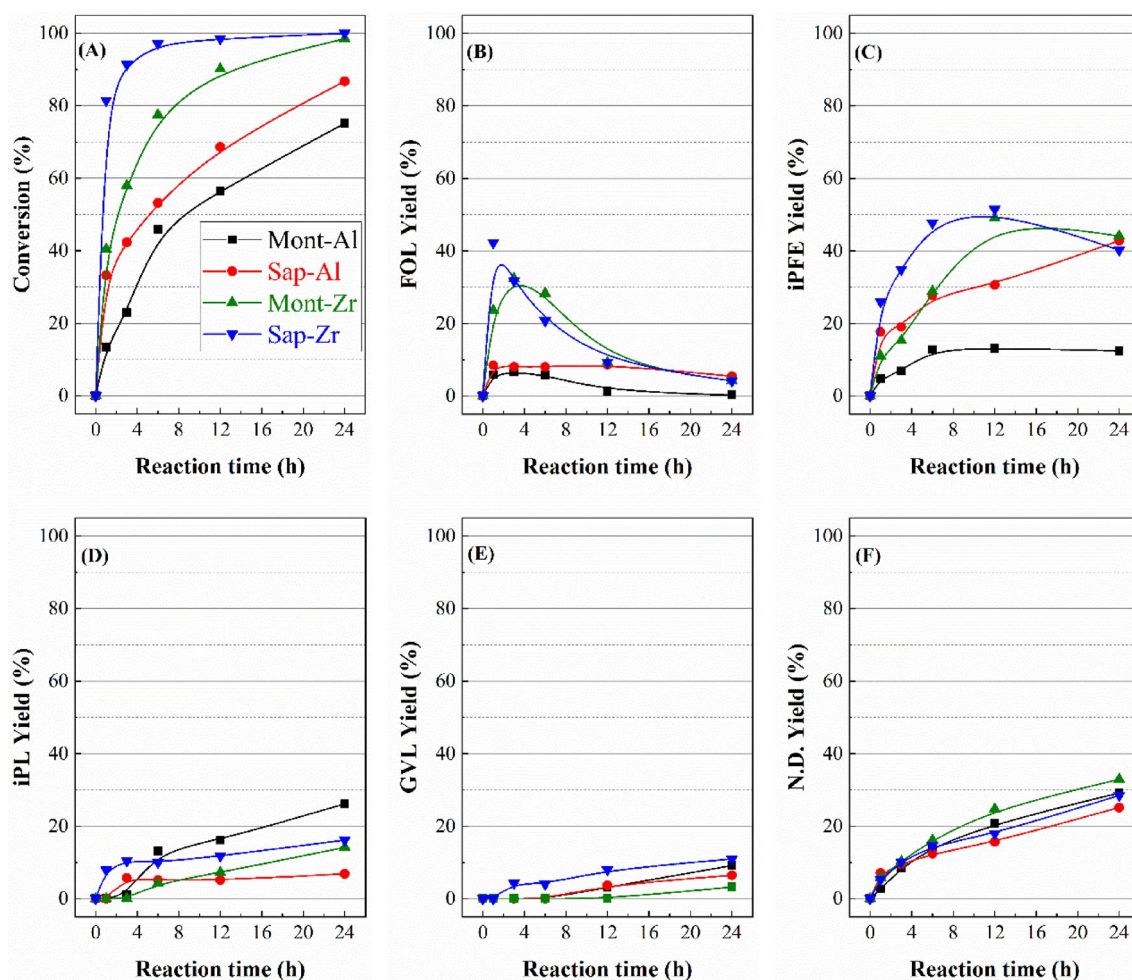


Fig. 9 FUR conversion (A), furfuryl alcohol, FOL (B), i-propyl furfuryl ether, iPFEE (C), i-propyl levulinate, iPL (D), γ -valerolactone, GVL (E) and non-detected products (F) yields in the one-pot reaction of FUR into valuable products using Mont-Al, Mont-Zr, Sap-Al and

Sap-Zr. (Experimental conditions: 0.1 g of catalyst, temperature reaction: 170 °C, reaction time: 0–24 h, iPOH/FUR molar ratio: 50, FUR/catalyst weight ratio: 1)

increases, except in the case of Mont-Zr, where FOL and iPFEE grew similarly. For the other catalysts, a drop in FOL yield and a concomitant increase in iPFEE yield was observed due to the etherification reaction of FOL with iPOH, in such a way that iPFEE is the main product at higher reaction

Table 4 Textural properties of the used catalysts after 6 h of reaction at 170 °C

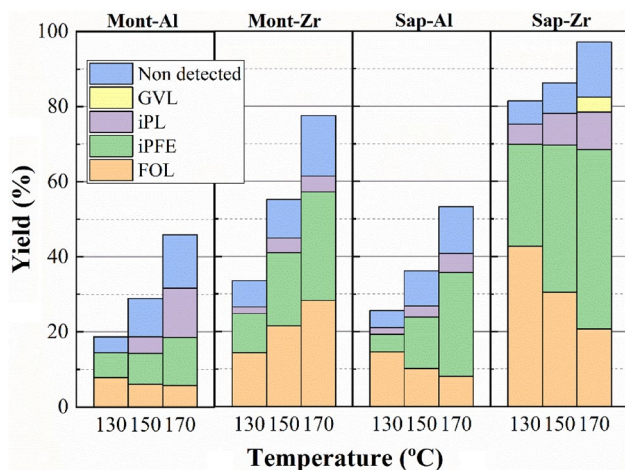
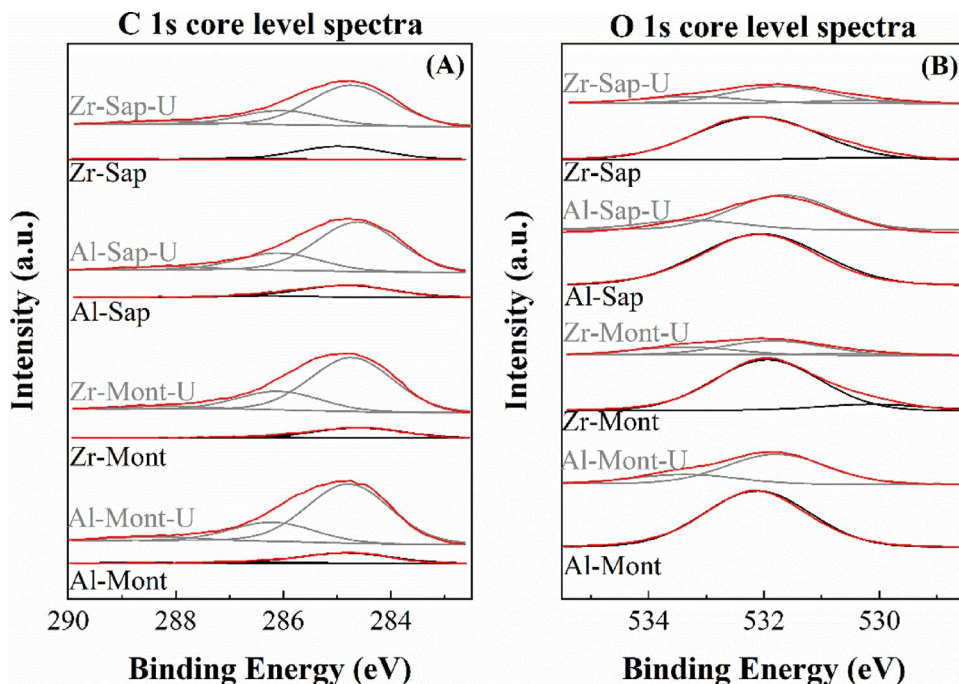
Sample	S_{BET} (m ² /g)	S_{MIC} (m ² /g)	V_{p} (cm ³ /g)	V_{MIC} (cm ³ /g)
Mont-U	18	1	0.0423	0.0003
Mont-Al-U	17	3	0.0289	0.0013
Mont-Zr-U	8	2	0.0145	0.0011
Sap-U	35	2	0.0613	0.0008
Sap-Al-U	19	1	0.0334	0.0003
Sap-Zr-U	10	2	0.0186	0.0006

temperature. In the same way, the formation of iPL is also favored at higher temperature [68]. However, these yields are relatively low compared to those of iPFEE, confirming that the reaction is retained in the furan ring opening regardless the reaction temperature due to the low proportion of Brønsted acid sites in the catalysts (Table 2). Finally, GVL is only observed in Sap-Zr catalyst, being expected due to the poor iPL yield attained in previous studies (Fig. 9). In addition, as previously noted, the lactonization reaction to form GVL requires high temperatures and longer reaction times. Moreover, the formation of non-detected products increases with the reaction temperature in all cases, confirming that the polymerization and undesired condensation are favored at higher temperatures.

In a final study, the reuse of the most active catalysts (Sap-Zr and Mont-Zr) was also evaluated (Fig. 12). In both catalysts, FUR conversion decays with the number of cycles

Table 5 Surface atomic composition of the used catalysts after 6 h of reaction at 170 °C

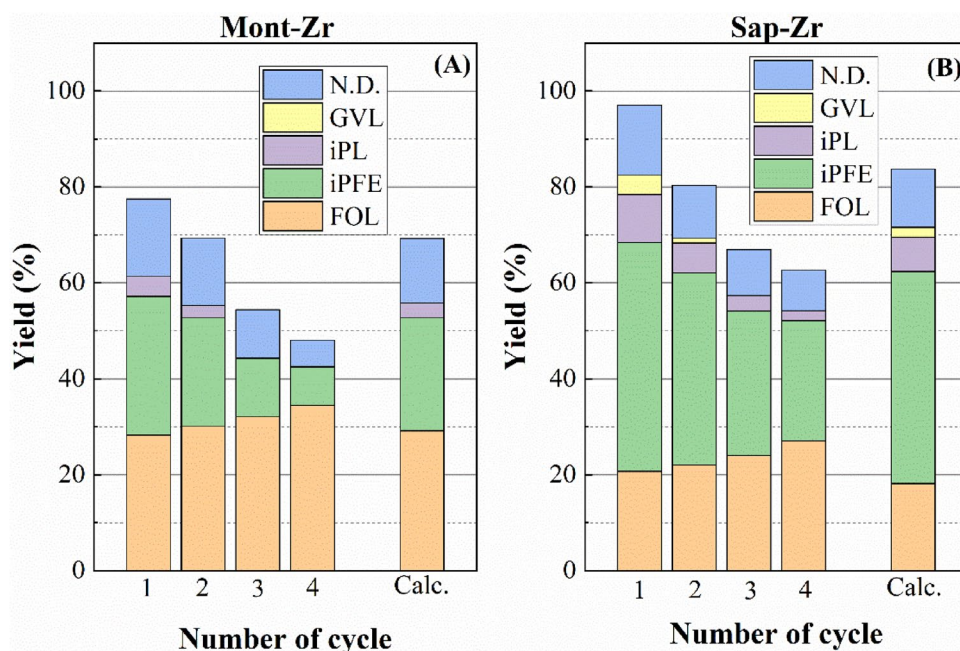
Sample	Atomic concentrations							
	C 1 s	O 1 s	Si 2p	Al 2p	Mg 1 s	Zr 3d	Na 1 s	Fe 2p
Mont-Al-U	47.1	39.5	7.6	4.6	0.5	–	0.2	0.6
Mont-Zr-U	58.6	32.6	5.0	1.7	0.1	1.3	0.2	0.5
Sap-Al-U	38.2	43.3	8.5	3.3	6.3	–	0.2	0.2
Sap-Zr-U	48.1	38.2	7.2	1.1	2.1	2.6	0.3	0.3

Fig. 10 Comparison of the C 1 s (A) and O 1 s (B) core level spectra, before and after the catalytic reaction at 170 °C for 24 h**Fig. 11** FUR conversion and yields for Mont-Al, Mont-Zr, Sap-Al and Sap-Zr between 130 and 170 °C. (Experimental conditions: 0.1 g of catalyst, reaction time: 6 h, iPOH/FUR molar ratio: 50, FUR/catalyst weight ratio: 1)

due to the formation of carbonaceous deposits on the catalyst surface, because of polymerization or condensation reactions of FUR or FOL. This implies an impoverish of the textural properties (Table 4 and Supplementary Information Figures S4 and S5), as well as a blockage of the acid sites involved in the one-pot process causing a progressive decay in the catalytic activity. Thus, Mont-Zr shows a decrease of FUR conversion from 78% after the 1st cycle to 40% after the 4th cycle, after 6 h at 170 °C in each cycle. In the case of Sap-Zr, a similar trend is observed, since the FUR yield decays from 98% after the 1st cycle to 62% after the 4th cycle. The regeneration of the catalyst by a thermal treatment at 550 °C for 6 h with air in static conditions causes a notable improvement of the catalytic performance, probably due to the removal of the carbonaceous deposits, reaching values close to those obtained after the 1st cycle. In this sense, the FUR conversion values are slightly below those obtained after the 1st cycle due to the loss of acid sites after the thermal treatment at 550 °C.

The profile of the obtained products also differs after each cycle. Thus, both iPL and iPFE yields progressively decrease after each cycle; however, the FOL yield enhances. In this

Fig. 12 Reuse of Mont-Zr and Sap-Zr catalysts. (Experimental conditions: 0.1 g of catalyst, temperature reaction: 170 °C, reaction time: 6 h, iPOH/FUR molar ratio: 50, FUR/catalyst weight ratio: 1)



sense, the blockage of acid sites retains the one-pot process in earlier steps, in such a way that the CTH reaction to form FOL is the main reaction. In contrast, the etherification and ring opening reactions are more limited due to the worsening of textural properties and blocking of active sites. The regeneration of the catalyst by calcination leads to a similar pattern of products in comparison to the 1st cycle, although it is not possible to recover the initial values.

5 Conclusions

Two smectites, montmorillonite and saponite, have been used as starting materials for the synthesis of pillared clays by the insertion of polyoxocations in the interlayer region and subsequent calcination. The presence of these polyoxocations causes a partial delamination of the clays, as well as an increase in the surface area and pore volume. In the same way, the insertion of Al_2O_3 and ZrO_2 promotes the formation of acid sites, generally of Lewis type, which are involved in the catalytic transfer hydrogenation to reduce aldehydes into alcohols. In the same way, the presence of a small proportion of Brønsted acid sites also promotes other reactions as the opening of the furanic ring, in such a way that consecutive reactions take place in this process.

The study of these samples in the one-pot process to convert FUR into valuable products reveals that Sap sample displays a higher conversion in comparison to Mont, probably due to its better textural properties (larger surface area and pore volume). The study of the pillared clays points out an improvement in the catalytic behavior, reaching full conversion at shorter reaction times, mainly in the case of the Zr-based

catalysts. Regarding the obtained products, the most active catalyst is Sap-Zr, showing the formation of a high proportion of FOL at short reaction times, with a maximum FOL yield of 42% after 1 h of reaction at 170 °C. However, longer reaction times provoke a decrease in FOL yield, while the formation of iPFE is favored notably, achieving iPFE yields close to 50% for Mont-Zr and Sap-Zr samples, after 12 h of reaction at 170 °C. On the other hand, it seems that the reactions are retained in the formation of iPFE, probably due to the low proportion of Brønsted acid sites involved in the one-pot process.

The reuse evaluation shows a notable decrease in the FUR conversion due to the formation of carbonaceous deposits along the reaction, causing a decrease in the surface area, pore volume, as well as the blockage of the acid sites. However, these catalysts can be regenerated by calcination, achieving conversion and yields close to those of the fresh catalysts.

Supplementary Information The online version contains supplementary material available at <https://doi.org/10.1007/s11244-024-01971-3>.

Acknowledgements This research was funded by Spanish Ministry of Science and Innovation (PID2021–122736OB-C42), FEDER (European Union) funds (PID2021–122736OB-C42, FQM-155, UMA20-FEDERJA-088). Moreover, F. Franco thanks Cátedra Ciencias del Litoral Costa del Sol (807/41.5223) for the financial support.

Funding Funding for open access publishing: Universidad Málaga/CBUA.

Data availability Raw data are available upon request.

Open Access This article is licensed under a Creative Commons Attribution 4.0 International License, which permits use, sharing, adaptation, distribution and reproduction in any medium or format, as long as you give appropriate credit to the original author(s) and the source, provide a link to the Creative Commons licence, and indicate if changes

were made. The images or other third party material in this article are included in the article's Creative Commons licence, unless indicated otherwise in a credit line to the material. If material is not included in the article's Creative Commons licence and your intended use is not permitted by statutory regulation or exceeds the permitted use, you will need to obtain permission directly from the copyright holder. To view a copy of this licence, visit <http://creativecommons.org/licenses/by/4.0/>.

References

- Kohli K, Prajapati R, Sharma BK (2019) Bio-based chemicals from renewable biomass for integrated biorefineries. *Energies* 12:233. <https://doi.org/10.3390/en12020233>
- Huber GW, Iborra S, Corma A (2006) Synthesis of transportation fuels from biomass: Chemistry, catalysts, and engineering. *Chem Rev* 106:4044–4098. <https://doi.org/10.1021/cr068360d>
- Ashokkumar V, Venkatkarthick R, Jayashree S, Chuetor S, Dharmaraj S, Kumar G, Chen WH, Ngamcharussrivichai C (2022) Recent advances in lignocellulosic biomass for biofuels and value-added bioproducts—a critical review. *Bioresour Technol* 344:126195. <https://doi.org/10.1016/j.biortech.2021.126195>
- Mäki-Arvela P, Salmi T, Holmbom B, Willför S, Murzin DY (2011) Synthesis of sugars by hydrolysis of hemicelluloses—a review. *Chem Rev* 111:5638–5666. <https://doi.org/10.1021/cr2000042>
- Delbecq F, Wang Y, Muralidhara A, El Ouardi K, Marlair G, Len C (2018) Hydrolysis of hemicellulose and derivatives—a review of recent advances in the production of furfural. *Front Chem* 6:146. <https://doi.org/10.3389/fchem.2018.00146>
- Mariscal R, Maireles-Torres P, Ojeda M, Sádaba I, López-Granados M (2016) Furfural: a renewable and versatile platform molecule for the synthesis of chemicals and fuels. *Energy Environ Sci* 9:1144–1189. <https://doi.org/10.1039/C5EE02666K>
- Lange JP, van der Heide E, van Buijtenen J, Price R (2012) Furfural - A promising platform for lignocellulosic biofuels. *ChemSuschem* 5:150–166. <https://doi.org/10.1002/cssc.201100648>
- Hoydonckx HE, van Rhijn WM, van Rhijn W, de Vos DE, Jacobs PA, Hoydonckx HE, van Rhijn WM, van Rhijn W, de Vos DE, Jacobs PA (2007) Furfural and Derivatives. *Ullmann's Encycl. Ind. Chem.*, Wiley-VCH Verlag GmbH & Co. KGaA, Weinheim, Germany. https://doi.org/10.1002/14356007.a12_119.pub2
- Yan K, Wu G, Lafleur T, Jarvis C (2014) Production, properties and catalytic hydrogenation of furfural to fuel additives and value-added chemicals. *Renew Sustain Energy Rev* 38:663–676. <https://doi.org/10.1016/j.rser.2014.07.003>
- García-Sancho C, Mérida-Robles JM, Cecilia-Buenestado JA, Moreno-Tost R, Maireles-Torres PJ (2023) The role of copper in the hydrogenation of furfural and levulinic acid. *Int J Mol Sci* 24:2443. <https://doi.org/10.3390/ijms24032443>
- Wang Y, Zhao D, Rodríguez-Padrón D, Len C (2019) Recent advances in catalytic hydrogenation of furfural. *Catalysts* 9:796. <https://doi.org/10.3390/catal9100796>
- Jiménez-Gómez CP, Cecilia JA, Moreno-Tost R, Maireles-Torres P (2017) Selective production of 2-methylfuran by gas-phase hydrogenation of furfural on copper incorporated by complexation in mesoporous silica catalysts. *ChemSuschem* 10:1448–1459. <https://doi.org/10.1002/cssc.201700086>
- Jiménez-Gómez CP, Cecilia JA, Alba-Rubio AC, Cassidy A, Moreno-Tost R, García-Sancho C, Maireles-Torres P (2022) Tailoring the selectivity of Cu-based catalysts in the furfural hydrogenation reaction: Influence of the morphology of the silica support. *Fuel* 319:123827. <https://doi.org/10.1016/j.fuel.2022.123827>
- Nakagawa Y, Nakazawa H, Watanabe H, Tomishige K (2012) Total hydrogenation of furfural over a silica-supported nickel catalyst prepared by the reduction of a nickel nitrate precursor. *ChemCatChem* 4:1791–1797. <https://doi.org/10.1002/cctc.201200218>
- Meng X, Yang Y, Chen L, Xu M, Zhang X, Wei M (2019) A control over hydrogenation selectivity of furfural via tuning exposed facet of Ni catalysts. *ACS Catal* 9:4226–4235. <https://doi.org/10.1021/acscatal.9b00238>
- Jiménez-Gómez CP, Cecilia JA, Moreno-Tost R, Maireles-Torres P (2017) Nickel phosphide/silica catalysts for the gas-phase hydrogenation of furfural to high-added-value chemicals. *ChemCatChem* 9:2881–2889. <https://doi.org/10.1002/cctc.201700312>
- Guerrero-Torres A, Jiménez-Gómez CP, Cecilia JA, García-Sancho C, Franco F, Quirante-Sánchez JJ, Maireles-Torres P (2019) Ni supported on sepiolite catalysts for the hydrogenation of furfural to value-added chemicals: influence of the synthesis method on the catalytic performance. *Top Catal* 62:535–550. <https://doi.org/10.1007/s11244-019-01168-z>
- Meerwein H, Schmidt R (1925) Ein neues verfahren zur reduktion von aldehyden und ketonen. *Liebigs Ann Chem* 444:221–238. <https://doi.org/10.1002/jlac.19254440112>
- Ponndorf W (1926) Der reversible austausch der oxydationsstufen zwischen aldehyden oder ketonen einerseits und primären oder sekundären alkoholen andererseits. *Angew Chem* 39:138–143. <https://doi.org/10.1002/ange.19260390504>
- Verley M (1925) The Exchange of functional groups between two molecules. The passage of ketones to alcohols and the reverse. *Bull Soc Chim Fr* 37:871–874
- Gilkey MJ, Xu B (2016) Heterogeneous catalytic transfer hydrogenation as an effective pathway in biomass upgrading. *ACS Catal* 6:1420–1436. <https://doi.org/10.1021/acscatal.5b02171>
- Hidalgo-Carrillo J, Parejas A, Cuesta-Rioboo MJ, Marinas A, Urbano FJ (2018) MPV reduction of furfural to furfuryl alcohol on Mg, Zr, Ti, Zr-Ti, and Mg-Ti solids: Influence of acid-base properties. *Catalysts* 8:539. <https://doi.org/10.3390/catal8110539>
- Maderuelo-Solera R, López-Asensio R, Cecilia JA, Jiménez-Gómez CP, García-Sancho C, Moreno-Tost R, Maireles-Torres P (2019) Catalytic transfer hydrogenation of furfural to furfuryl alcohol over calcined MgFe hydroxalicates. *Appl Clay Sci* 183:105351. <https://doi.org/10.1016/j.clay.2019.105351>
- Ooi T, Miura T, Itagaki Y, Ichikawa H, Maruoka K (2002) Catalytic Meerwein-Ponndorf-Verley (MPV) and Oppenauer (OPP) reactions: Remarkable acceleration of the hydride transfer by powerful bidentate aluminum alkoxides. *Synthesis* 2:279–291. <https://doi.org/10.1055/s-2002-19802>
- Liu YC, Ko BT, Huang BH, Lin CC (2002) Reduction of aldehydes and ketones catalyzed by a novel aluminum alkoxide: mechanistic studies of Meerwein-Ponndorf-Verley reaction. *Organometallics* 21:2066–2069. <https://doi.org/10.1021/om200454>
- López-Asensio R, Cecilia JA, Jiménez-Gómez CP, García-Sancho C, Moreno-Tost R, Maireles-Torres P (2018) Selective production of furfuryl alcohol from furfural by catalytic transfer hydrogenation over commercial aluminas. *Appl Catal A* 556:1–9. <https://doi.org/10.1016/j.apcata.2018.02.022>
- García-Sancho C, Jiménez-Gómez CP, Viar-Antuñano N, Cecilia JA, Moreno-Tost R, Mérida-Robles JM, Requies J, Maireles-Torres P (2021) Evaluation of the ZrO₂/Al₂O₃ system as catalysts in the catalytic transfer hydrogenation of furfural to obtain furfuryl alcohol. *Appl Catal A* 609:117905. <https://doi.org/10.1016/j.apcata.2020.117905>
- Montes V, Miñambres JF, Khalilov AN, Boutonnet M, Marinas JM, Urbano FJ, Maharramov AM, Marinas A (2018) Chemoselective hydrogenation of furfural to furfuryl alcohol on ZrO₂ systems synthesized through the microemulsion method. *Catal Today* 306:89–95. <https://doi.org/10.1016/j.cattod.2017.05.022>

29. Komanoya T, Nakajima K, Kitano M, Hara M (2015) Synergistic catalysis by Lewis acid and base sites on ZrO₂ for Meerwein-Ponndorf-Verley reduction. *J Phys Chem C* 119:26540–26546. <https://doi.org/10.1021/acs.jpcc.5b08355>
30. Akinawo CA, Bingwa N, Meijboom R (2021) Surface properties vs activity of meso-ZrO₂ catalyst in chemoselective Meerwein-Ponndorf-Verley reduction of citral: effect of calcination temperature. *Micropor Mesopor Mater* 311:110693. <https://doi.org/10.1016/j.micromeso.2020.110693>
31. López-Asensio R, Jiménez-Gómez CP, García-Sancho C, Moreno-Tost R, Cecilia JA, Maireles-Torres P (2019) Influence of structure-modifying agents in the synthesis of Zr-doped SBA-15 silica and their use as catalysts in the furfural hydrogenation to obtain high value-added products through the Meerwein-Ponndorf-Verley reduction. *Int J Mol Sci* 20:828. <https://doi.org/10.3390/ijms20040828>
32. Maderuelo-Solera R, Richter S, Jiménez-Gómez CP, García-Sancho C, García-Mateos FJ, Rosas JM, Moreno-Tost R, Cecilia JA, Maireles-Torres P (2021) Porous SiO₂ nanospheres modified with ZrO₂ and their use in one-pot catalytic processes to obtain value-added chemicals from furfural. *Ind Eng Chem Res* 60:18791–18805. <https://doi.org/10.1021/acs.iecr.1c02848>
33. Iglesias J, Melero JA, Morales G, Moreno J, Segura Y, Paniagua M, Cambra A, Hernández B (2015) Zr-SBA-15 Lewis acid catalyst: activity in Meerwein Ponndorf Verley reduction. *Catalysts* 5:1911–1927. <https://doi.org/10.3390/catal5041911>
34. Iglesias J, Melero JA, Morales G, Paniagua M, Hernández B, Osatiashtiani A, Lee AF, Wilson K (2018) ZrO₂-SBA-15 catalysts for the one-pot cascade synthesis of GVL from furfural. *Catal Sci Technol* 8:4485–4493. <https://doi.org/10.1039/C8CY01121D>
35. Melero JA, Morales G, Iglesias J, Paniagua M, López-Aguado C (2018) Rational optimization of reaction conditions for the one-pot transformation of furfural to γ -valerolactone over Zr–Al-beta zeolite: Toward the efficient utilization of biomass. *Ind Eng Chem Res* 57:11592–11599. <https://doi.org/10.1021/acs.iecr.8b02475>
36. Boronat M, Corma A, Renz M (2006) Mechanism of the Meerwein-Ponndorf-Verley-Oppenauer (MPVO) redox equilibrium on Sn- and Zr-Beta zeolite catalysts. *J Phys Chem B* 110:21168–21174. <https://doi.org/10.1021/jp063249x>
37. Zhu Y, Chuah GK, Jaenicke S (2006) Selective Meerwein-Ponndorf-Verley reduction of α , β -unsaturated aldehydes over Zr-zeolite beta. *J Catal* 241:25–33. <https://doi.org/10.1016/j.jcat.2006.04.008>
38. Gonell F, Boronat M, Corma A (2017) Structure-reactivity relationship in isolated Zr sites present in Zr-zeolite and ZrO₂ for the Meerwein-Ponndorf-Verley reaction. *Catal Sci Technol* 7:2865–2873. <https://doi.org/10.1039/C7CY00567A>
39. Wang J, Okamura K, Jaenicke S, Chuah GK (2015) Post-synthesized zirconium-containing Beta zeolite in Meerwein-Ponndorf-Verley reduction: Pros and cons. *Appl Catal A* 493:112–120. <https://doi.org/10.1016/j.apcata.2015.01.001>
40. Khoele M, Lobo RF (2016) Lewis acidic zeolite Beta catalyst for the Meerwein-Ponndorf-Verley reduction of furfural. *Catal Sci Technol* 6:3018–3026. <https://doi.org/10.1039/C5CY01501D>
41. Valekar AH, Lee M, Yoon JW, Kwak J, Hong DY, Oh KR, Cha GY, Kwon YU, Jung J, Chang JS, Hwang YK (2020) Catalytic transfer hydrogenation of furfural to furfuryl alcohol under mild conditions over Zr-MOFs: Exploring the role of metal node coordination and modification. *ACS Catal* 10:3720–3732. <https://doi.org/10.1021/acscatal.9b05085>
42. Zhang P, Hou P, Ma M, Bu K, Guo Q, Yue H, Tian G, Feng S (2023) Bifunctional zirconium-based metal-organic frameworks as chemoselective catalysts for the synthesis of γ -valerolactone from furfural via a one-pot cascade reaction. *Appl Catal A* 653:119064. <https://doi.org/10.1016/j.apcata.2023.119064>
43. Wang Y, Huang J, Lu S, Lei P, Xia X, Li C, Li F (2020) Phosphorus-modified zirconium metal organic frameworks for catalytic transfer hydrogenation of furfural. *New J Chem* 44:20308–20315. <https://doi.org/10.1039/D0NJ04285D>
44. Yang J, Zhang Y, Shen F, Qi X (2023) Glucose-derived zirconium-containing mesoporous composite for efficient catalytic transfer hydrogenation of furfural to furfuryl alcohol. *Biomass Bioenergy* 170:106723. <https://doi.org/10.1016/j.biombioe.2023.106723>
45. Liu Y, Huang R, Zhang J, He L, Peng L (2021) Design of a multifunctional zirconium-based hybrid with natural lignocellulose for transfer hydrogenation of furfural to furfuryl alcohol. *Energy Fuels* 35:20231–20242. <https://doi.org/10.1021/acs.energyfuels.1c03109>
46. Zhang T, Lu Y, Li W, Su M, Yang T, Agunbiyi A, Jin Y (2019) One-pot production of γ -valerolactone from furfural using Zr-graphitic carbon nitride/H- β composite. *Int J Hydrogen Energy* 44:14527–14533. <https://doi.org/10.1016/j.ijhydene.2019.04.059>
47. Bergaya F, Aouad A, Mandalia T (2006) Pillared clays and clay minerals. *Develop Clay Miner* 1:393–421. [https://doi.org/10.1016/S1572-4352\(05\)01012-3](https://doi.org/10.1016/S1572-4352(05)01012-3)
48. Brindley GW, Sempels RE (1977) Preparation and properties of some hydroxy-aluminium beidellites. *Clay Miner* 12:229–237. <https://doi.org/10.1180/claymin.1977.012.3.05>
49. Issaadi R, Garin F, Chitour CE, Maire G (2001) Catalytic behaviour of combined palladium-acid catalysts: use of Al and Zr-pillared montmorillonite as supports: part I. Reactivity of linear, branched and cyclic hexane hydrocarbons. *Appl Catal A* 207:323–332. [https://doi.org/10.1016/S0926-860X\(00\)00664-5](https://doi.org/10.1016/S0926-860X(00)00664-5)
50. Martínez-Ortiz MJ, Fetter G, Domínguez JM, Melo-Banda JA, Ramos-Gómez R (2003) Catalytic hydrotreating of heavy vacuum gas oil on Al- and Ti-pillared clays prepared by conventional and microwave irradiation methods. *Micropor Mesopor Mater* 58:73–80. [https://doi.org/10.1016/S1387-1811\(02\)00592-9](https://doi.org/10.1016/S1387-1811(02)00592-9)
51. Bartley GJJ (1988) Zirconium pillared clays. *Catal Today* 2:233–241. [https://doi.org/10.1016/0920-5861\(88\)85006-5](https://doi.org/10.1016/0920-5861(88)85006-5)
52. Cecilia JA, Pardo L, Pozo M, Bellido E, Franco F (2018) Microwave-assisted acid activation of clays composed of 2:1 clay minerals: a comparative study. *Minerals* 8:376. <https://doi.org/10.3390/min8090376>
53. Occelli ML (1988) Surface properties and cracking activity of delaminated clay catalysts. *Catal Today* 2:339–355. [https://doi.org/10.1016/0920-5861\(88\)85014-4](https://doi.org/10.1016/0920-5861(88)85014-4)
54. Zviagina BB, McCarty DK, Srodon J, Drits VA (2004) Interpretation of infrared spectra of dioctahedral smectites in the region of OH-stretching vibrations. *Clays Clay Miner* 52:399–410. <https://doi.org/10.1346/CCMN.2004.0520401>
55. Franco F, Pozo M, Cecilia JA, Benítez-Guerrero M, Lorente M (2016) Effectiveness of microwave assisted acid treatment on dioctahedral and trioctahedral smectites. The influence of octahedral composition. *Appl Clay Sci* 120:70–80. <https://doi.org/10.1016/j.clay.2015.11.021>
56. Madejová J (2003) FTIR techniques in clay mineral studies. *Vib Spectrosc* 31:1–10. [https://doi.org/10.1016/S0924-2031\(02\)00065-6](https://doi.org/10.1016/S0924-2031(02)00065-6)
57. Marques Correia L, Cecilia JA, Rodríguez-Castellón E, Cavalcante CL (2017) Silveira Vieira (2017) Relevance of the physicochemical properties of calcined quail eggshell (CaO) as a catalyst for biodiesel production. *J Chem* 1:1–12. <https://doi.org/10.1155/2017/5679512>
58. Thommes M, Kaneko K, Neimark AV, Olivier JP, Rodríguez-Reinoso F, Rouquerol J, Sing KSW (2015) Physisorption of gases, with special reference to the evaluation of surface area and pore

- size distribution (IUPAC Technical Report). *Pure Appl Chem* 87:1051–1069. <https://doi.org/10.1515/pac-2014-1117>
59. Brunauer S, Emmett PH, Teller E (1938) Adsorption of gases in multimolecular layers. *J Am Chem Soc* 60:309–319. <https://doi.org/10.1021/ja01269a023>
 60. Corma A, Rodellas C, Fornes V (1984) Characterization of acid surfaces by adsorption of 2,6-dimethylpyridine. *J Catal* 88:374–381. [https://doi.org/10.1016/0021-9517\(84\)90014-9](https://doi.org/10.1016/0021-9517(84)90014-9)
 61. Peng Q, Wang H, Xia Y, Liu X (2021) One-pot conversion of furfural to gamma-valerolactone in the presence of multifunctional zirconium alizarin red S hybrid. *Appl Catal A* 621:118203. <https://doi.org/10.1016/j.apcata.2021.118203>
 62. Kim KD, Kim J, Teoh WY, Kim JC, Huang J, Ryoo R (2020) Cascade reaction engineering on zirconia-supported mesoporous MFI zeolites with tunable Lewis-Brønsted acid sites: a case of the one-pot conversion of furfural to γ -valerolactone. *RSC Adv* 10:35318–35238. <https://doi.org/10.1039/D0RA06915A>
 63. Miñambres JF, Cejka J (2023) Meerwein-Ponndorf-Verley reduction in current heterogeneous catalysis research: a review. *Catal Rev*. <https://doi.org/10.1080/01614940.2023.2197716>
 64. Filicetto L, Balu AM, Van der Waal J, Luque R (2018) Catalytic insights into the production of biomass-derived side products methyl levulinate, furfural and humins. *Catal Today* 302:2–15. <https://doi.org/10.1016/j.cattod.2017.03.008>
 65. Liu S, Zhu Y, Liao Y, Wang H, Liu Q, Ma L, Wang C (2022) Advances in understanding the humins: formation, prevention and application. *Appl Energy Combust Sci* 10:100062. <https://doi.org/10.1016/j.jaecs.2022.100062>
 66. Di Carmine G, Leonardi C, Forster L, Hu M, Lee D, Parlett CMA, Bortoloni O, Isaacs MA, Massi A, D'Agostino C (2023) Humin formation on SBA-15-pr-SO₃H catalysts during the alcoholysis of furfuryl alcohol to ethyl levulinate: effect of pore size on catalyst stability, transport, and adsorption. *ACS Appl Mater Interfaces* 15:24528–24540. <https://doi.org/10.1021/acsami.3c04613>
 67. Chatterjee A, Hu X, Lam FLY (2019) Modified coal fly ash waste as an efficient heterogeneous catalyst for dehydration of xylose to furfural in biphasic medium. *Fuel* 239:726–736. <https://doi.org/10.1016/j.fuel.2018.10.138>
 68. Gómez-Bernal H, Benito P, Rodríguez-Castellón E, Raspolli Galletti AM, Funaioli T (2019) Synthesis of isopropyl levulinate from furfural: Insights on a cascade production perspective. *Appl Catal A* 575:111–119. <https://doi.org/10.1016/j.apcata.2019.02.018>

Publisher's Note Springer Nature remains neutral with regard to jurisdictional claims in published maps and institutional affiliations.